STABILITY, MECHANICAL CONSIDERATIONS, AND AC LOSS IN HTSC MONOLITHS, COILS, AND WIRES

M. D. Sumption and E. W. Collings

Battelle Memorial Institute
505 King Ave, Columbus, OH 43201, USA

Abstract

For monolithic high-T_c superconductors (HTSCs) calculations are presented of: (1) the initial flux jump field, H_{fj}, in melt-processed YBCO based on a field- and temperature dependent J_c, and (2) the radial and circumferential stresses in solid and hollow cylinders containing trapped magnetic flux. For model multifilamentary (MF) HTSC/Ag strands calculations are presented of: (1) the limiting filament diameters for adiabatic and dynamic stability, and (2) the hysteretic and eddy current components of AC loss. Again for MF HTSC/Ag composite strands the need for filamentary subdivision and twisting is discussed.

INTRODUCTION

Large-scale applications of high-T_c superconductors (HTSCs) stem not only from their obviously high T_cs which offer the possibility of operation in liquid hydrogen, liquid nitrogen as well as refrigerated gases, but also from their high H_{c2}s when high operating temperature is not the primary consideration. The thermal properties central to stable conductor design are thermal conductivity, K(T), and specific heat, C(T). The former dominates at low temperatures and there dictates the choice of a dynamic stability criterion. Specific heat takes over at high temperatures where stability is controlled by adiabatic considerations. The much higher C(T) of materials at 77 K than at 4 K guarantees a much greater adiabatic flux-jump stability. Several effects related to stability, while present in LTSC materials, are much more prominent in HTSCs; for example, a much more pronounced ramp rate dependence of flux jumping (in non-stabilized samples).[1] In the first section of this paper, the field dependence of flux jumping in large monoliths of HTSC, and its associated adiabatic and dynamic aspects, will be considered. In the next section we calculate the Lorentz-force induced mechanical stresses that are present in flux-trapped solid cylinders of melt grown YBCO. We then go on to compare these results to those for hollow cylinders. The discussion on stability then concludes with a note on flux-jump- and cryo-stabilization of Ag-clad HTSC strands. The paper continues with a discussion of AC loss in multifilamentary HTSC/Ag composite strands. Using a model strand configuration, typical hysteretic and eddy current losses are compared with reference to practically attainable matrix resistivities and twist pitches. We conclude with a discussion of the particular properties of filamentary subdivision in HTSCs.

MAGNETIC STABILITY OF HTSC MONOLITHS

A well known expression for the initial flux jump field, is $H_{j0} = \sqrt{\{\pi^3 C(T)\Delta T_0\}}$, in which $\Delta T_0 \equiv J_c/(-dJ_c/dT)$. In its more widely used form, in which ΔT_0 is replaced by (T_c-T_b), a number of assumptions have been made: (1) J_c is linearly dependent on T, (2) J_c is field independent, and (3) the sample is isotropic. These assumptions are convenient, and have worked reasonably

well for LTSCs. However, Müller and Andrikidis[2] have recently developed an expression which takes into account the field dependence of J_c based on the Kim model, $J_c = J_{c0}H_0/(H+H_0)$. Field dependence of J_c has been considered before, both experimentally[3] and theoretically using a Kim-type model[4], although Müller et al.'s treatment[2] is the most complete.

Müller et al.'s expression for this modified flux jump field for a semi-infinite slab on the virgin run is given implicitly by

$$2\left[(|H_{fj}| - |H_e|)(|H_{fj}| + H_0) + (|H_{fj}| + H_0)(|H_e| + H_0)Ln\left(\frac{H_0 + |H_e|}{H_0 + |H_{fj}|}\right)\right] = H_{j0}^2 \qquad (1)$$

Here H_{fj} is the new flux jump field, H_e is an internal field due to previous flux jumps (we will set it to zero), and H_0 is the Kim model parameter. Curves derived from this expression in case (i) $\mu_0H_0 = \infty$ ($H_{fj} \equiv H_{j0}$), (ii) $\mu_0H_0 = 4$ T and (iii) $\mu_0H_0 = 0.1$ T are plotted in Fig. 1. We have chosen to plot H_{fj} for the virgin run, where we additionally require $H_e = 0$, since it does not involve the past history of the sample, and is easily compared to experimental results. Following Müller et al., in calculating Fig. 1 we assembled previously published[5] specific heat data from two temperature ranges -- 1-17 K and 30-100 K -- extrapolating them both to 26 K to complete the data set. This causes a discontinuity in slope of C(T) at 26 K and hence in the slope of the resulting H_{fj}.

It is noteworthy that the temperature dependence of H_{fj} responds strongly to the choice of the Kim field, H_0. It is also expected that the temperature dependence of J_c will also have a strong influence. We have noted from an inspection of several data sets for melt-processed YBCO that the combined temperature- and field dependence of J_c can be expressed in the form $J_c(T,H) = J_{c00}\exp(-T/T_s)H_0(T)/\{H_0(T)+H\}$. In particular, based on data from Maley et al.[6], we have deduced for their sample that $J_{c00} = 5.92 \times 10^5$ A/cm^2, $T_s = 19.87$ K, and $H_0(T) = a\text{-}bT$ (with $a = 2.504$ tesla, $b = 2.79\times10^{-2}$ tesla/K).

Ignoring for a moment the field dependence, the exponential form of $J_c(T)$ yields $\Delta T_0 = T_s$, leading to a "field-independent" H_{fj} of the form $\sqrt{\{\pi^3C(T)T_s\}}$. Next, an H_{fj} combining both J_c's exponential T-dependence and H_0's linear T-dependence was calculated. The new curve, also plotted in Fig. 1, covers just the region of exponentially fitted J_c data (up to about 80 K); at higher temperatures, J_c must decrease to zero more rapidly -- linearly would be a good approximation. The unusual shape of the final curve indicates that H_{fj} is sensitive to the full T-dependence of J_c. Indeed, in one of the first published papers on flux jumping, just such an effect was taken into account.[3] Given the wide temperature range over which HTSCs operate, and the wide variation in materials properties within it, inclusion of a T dependence as well as an H dependence is important for a quantitative description of flux jumping.

An interesting offshoot of the use of Kim-model-J_c field dependence is the prediction of a new flux jump regime -- that of the solitary flux jump. Flux jumping will occur when the field (or for a given d, J_c) becomes large enough. In the Bean model this can happen with equal likelihood anywhere around the M-H loop. However, for a Kim-type model, J_c (and thus field gradients) will be larger in some parts of the M-H loop than in others. In particular, two points on a Kim-type M-H loop which occur on the shielding branches, at relatively low fields (on opposite sides of the M-axis) have maximum overall field gradients. If we imagine following the trace of an M-H loop, once a flux jump is initiated at these high H-gradient

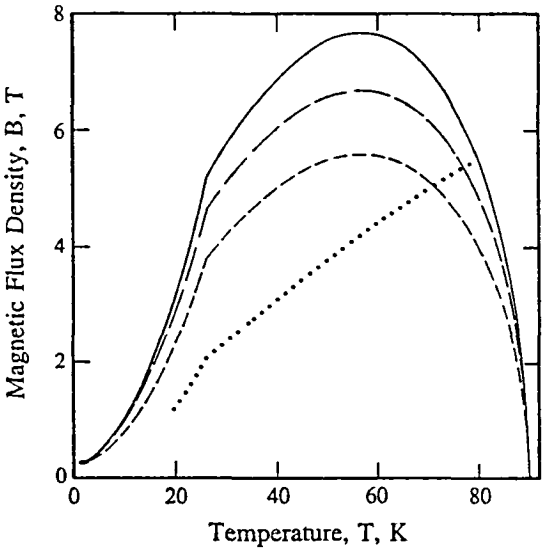

Figure 1. H_{fj} and H_{j0} vs T calculated for $\mu_0 H_0 = \infty$ (H_{j0}) (——), $\mu H_0 = 4$ T (— —), and $\mu H_0 = 0.1$ T (– – – –). Also shown is the result for $H_{fj} = H_{fj}$ (H,T) (• • • •, see text).

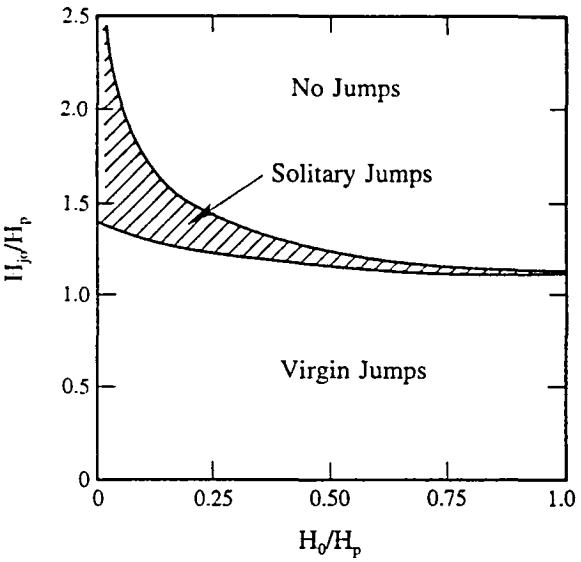

Figure 2. Illustration of the flux jump regimes. H_{j0}/H_p vs H_0/H_p for H_m/H_p =1, where H_p is the penetration field and H_m is the maximum field sweep amplitude. After Müller and Andrikidis.[2]

points, the total field difference is reduced. As H is increased (as we continue to sweep out the loop) the gradient cannot build back to its previously high value, since $J_c(H)$ is lower. We can then see that M-H loops executed in a certain range of temperature, and for certain H_0 values will exhibit pairs of "solitary" flux jumps. At lower temperatures, or as $H_0 \rightarrow \infty$, multiple flux jumps will occur (corresponding to the usual case). The solitary and multiple flux jumps regimes are displayed in Fig. 2. We note that the partial flux jump boundaries displayed in Fig. 1 will be extended somewhat by the solitary flux jump regime.

Another important idea which needs to be incorporated into the analysis of flux trapping samples is the influence of cooling on flux jump stability. It has been asserted that for slower ramp rates the ramp rate sensitivity of H_{fj} may be modified by dynamic cooling.[2] It seems clear that significant cooling will also occur along a direction orthogonal to the dimension along which the flux gradient is formed for flux trapping samples.[7] This suggests that the employment of a thin disk geometry may improve the stability of such samples.

It is also important to account for sample anisotropy. If H is parallel to c, then the problem is essentially isotropic. However, with H perpendicular to c, the stability will presumably be determined by the weaker of $H_{fj,a\text{-}b}$ and $H_{fj,c}$. However, this question has not been directly addressed.

STRESSES IN MELT GROWTH CYLINDERS AND POTTED MAGNETS ARISING FROM LORENTZ FORCES.

We have calculated the stress for a cylindrical superconductive sample used for flux trapping. While the literature concerning stresses in superconducting solenoids is extensive, we are unaware of any solutions for solid cylinders. This type of sample is shown in Fig. 3(a), with the field applied along the z-direction. Field independent J_c is assumed, and we have set the crystalline c-axis to be along the z-axis as well, in order to describe the configuration of

interest for flux trapping superconductors. Superconductive and mechanical properties will then be θ-invariant. We calculate the stresses after the sample has been set up in the full flux trapping state (presumably by field cooling), with the resultant flux profile shown in Fig. 3(b). The Lorentz force is given by $F = B_z J_c/10$ (in cgs-practical units). Using $dB/dr = 4\pi J_c/10$, the Lorentz force can be re-expressed as a function of position in the sample as

$$F(r) = \frac{4\pi J_c^2}{100}(R - r). \tag{2}$$

Following the procedure used to calculate the solenoidal solution[8,9], we start with the conditions of equilibrium for a 2-D θ-invariant problem in polar coordinates:

$$\frac{\partial}{\partial r}\sigma_r(r) + \frac{\sigma_r(r) - \sigma_\theta(r)}{r} + F(r) = 0. \tag{3}$$

The problem is similar to that of the spinning disk as described by Timoshenko.[10] Using his method we find the following expressions for the radial and circumferential (hoop) stress components, σ_r and σ_θ:

$$\sigma_r = \frac{1}{3}N_c R(2 + \nu)[R - r] - \frac{1}{8}N_c(3 + \nu)[R^2 - r^2],$$
$$\sigma_\theta = \frac{1}{3}N_c R(2 + \nu)R - \frac{1}{3}N_c R(1 + 2\nu)r - \frac{1}{8}N_c(3 + \nu)R^2 + \frac{1}{8}N_c(1 + 3\nu)r^2. \tag{4}$$

It can be shown that these expressions satisfy Eqn. 3, above. In cgs-practical units, $N_c = 4\pi J_c^2/100$, while in SI it is $\mu_0 J_c^2$. We have applied the boundary condition that $\sigma_r = 0$ at r = R. σ_r and σ_θ are shown as a function of r in Fig. 4 for a sample with R = 1.27 cm and $J_c = 10^9$ A/m^2. σ_θ drops monotonically with r to $(N_c R^2/12)(1-\nu)$ at the sample perimeter. σ_r, however,

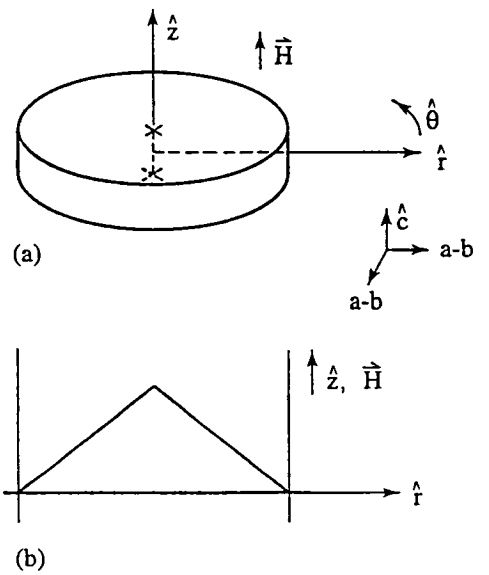

Figure 3. (a) Superconducting monolith with H‖c, and (b) Flux trapping profile.

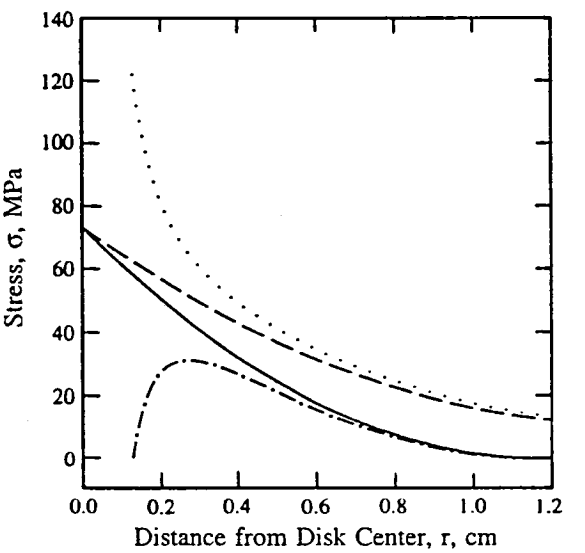

Figure 4. σ_r and σ_θ vs r for a solid superconducting disk (——σ_r, — —σ_θ), as well as one with a circular hole (—·—σ_r,·····σ_θ). Cylinder radius, R = 1.27 cm; hole radius, a = R/10; $J_c = 10^5$A/cm^2.

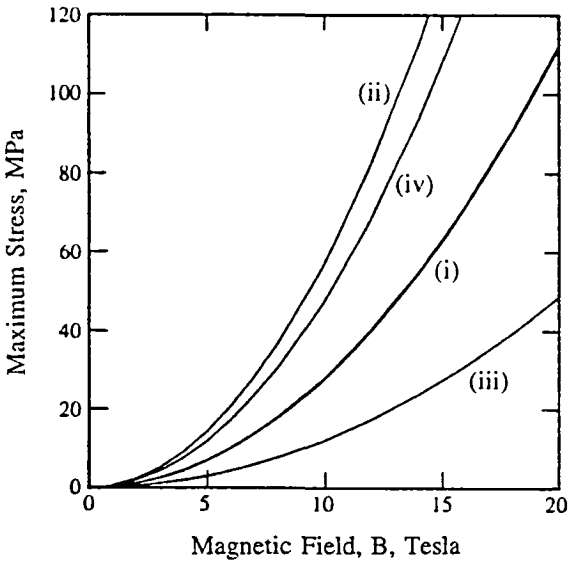

Figure 5. Maximum stresses for solid and axially perforated superconducting cylinders as functions of the maximum field (field at the center). (i) σ_r and σ_θ for the solid cylinder and σ_r for the axial pin-hole ($a/R = 10^{-5}$) cylinder; (ii) σ_θ for the latter; (iii) and (iv) σ_r and σ_θ, respectively, for the axially bored ($a/R=10^{-1}$) cylinder.

has a minimum at $r = (8/9)R(1 + \nu/2)/(1 + \nu/3)$, and σ_r is negative in this region. Physically this represents the action of the hoop stresses set up in the outermost regions of the cylinder. At $r = 0$, σ_r and σ_θ are maximum and equal; they are given by

$$\sigma_{max} = \frac{\pi J_c^2 R^2}{600}(7 + 5\nu) \tag{5}$$

in cgs-practical units (A/cm^2, cm, dyn/cm^2). To convert to SI units (A/m^2, m, Pa) multiply the right hand side of Eqn. 5 by $100\mu_0/4\pi$ (= 10^{-5}, numerically).

Substituting $\nu = 0.3$ in Eqn. 5 we find the maximum stress in the cylinder to be given by $\sigma_{max} \approx 0.35\mu_0 J_c^2 R^2$, which can be re-written in terms of maximum ($r = 0$) field, as $\sigma_{max} = 0.282\ B_{max}^2$. For these last expressions it is convenient to use SI units where B_{max} is in tesla and σ_{max} is in MPa. This relation is shown in Fig. 5. The tensile strength of polycrystalline YBCO is about 15 MPa, while for a single crystal, it is closer to 60 MPa.[11] This translates into a maximum field of 14.5 T for crystalline YBCO, which is above the quench field at any temperature (see above). If, as an approximation, we set the tensile strength of any grain boundaries which might be present in this material to 15 MPa (that of the sintered material), then the maximum field is 7.29 T. This is only somewhat lower than the maximum quench field (≈10 T), and it is only exceeded by H_{fj} in a small region near 60 K (under certain assumptions). We may therefore expect that mechanical integrity is not a problem for these flux trapping superconductors. However, the strains associated with the stress values listed above may well degrade J_c, although we have not yet considered this.

Next we go on to consider the same sample, but with an axial hole of radius a. The boundary conditions in this case are $\sigma_r = 0$ at $r = a$ and $r = R$. For the case of superconducting solenoids, Wilson[9] has developed an expression analogous to those above. If $J_{eff} = J_c$, these expressions can be re-written for comparison to the monolithic case as

$$\sigma_r(r,a,R) = \sigma_r(a=0) + \sigma_{add}$$

$$\sigma_\theta(r,a,R) = \sigma_\theta(a=0) + \sigma_{add} \tag{6}$$

where

$$\sigma_{add} = \frac{1}{3}N_c(2 + \nu)\left(\frac{Ra^2}{R + a}\right)\left[1 - q\frac{R^2}{r^2}\right] - \frac{1}{8}N_c(3 + \nu)a^2\left[1 - q\frac{R^2}{r^2}\right]$$

where q = 1 for σ_r and q = -1 for σ_θ. In the above treatment, hollow cylinders and potted Bi:HTSC/Ag pancake coils give the same results as solenoids. Plots for σ_r and σ_θ for a = R/10 are shown in Fig. 4 for comparison to the results for the monolith. We can see that the presence of the hole decreases σ_r, but increases σ_θ. In Fig. 5, curves of maximum σ_r and σ_θ (for a given internal B) are shown as a function of the internal field, B (which is assumed constant throughout the hole) and compared to the monolith results. For the case with the center hole, σ_θ still maximizes at the inner boundary, but σ_r maximizes somewhere within the structure, as shown in Fig. 4. As we can see in Figs. 4 and 5, with the introduction of a hole, σ_r becomes equal to or less than its counterpart for the monolith, while σ_θ becomes equal to or greater than its counterpart for the monolith. Thus, as shown in Fig. 5, in the limit of $a \rightarrow 0$, the maximum in $\sigma_{r,hole}$ is equal to the maximum value of $\sigma_{r,mono}$, while the maximum in $\sigma_{\theta,hole}$ is twice that of $\sigma_{\theta,mono}$. This agrees with the idea of stress enhancement around holes typically found in mechanics.

STABILITY IN MULTIFILAMENTARY STRANDS

Superconducting wires (strands) are generally produced in multifilamentary (MF) form. Low-T_c strands for accelerator magnet applications, for example, often consist of many thousands of filaments (e.g. 5,000 to 40,000); they are small in diameter to provide stability and low hysteretic loss, and twisted together to reduce eddy current loss to some fraction of the hysteretic value. As we shall see, in HTSC strands filamentary subdivision serves some of the above functions but also some additional ones. For practical reasons the number of filaments tends to be smaller and consequently the twisting requirement is less stringent. The first requirement in MF strand design is to prevent flux jumping. For NbTi, filaments smaller than about 100 μm in diameter are immune to it. This is also approximately true for HTSC strands at 4 K. But at 77 K they are adiabatically flux jump stable in diameters as large as several cm. In general, requirements other than stability tend to dictate the choice of filament diameter. For LTSCs these are low magnetization and low AC loss. For HTSCs the dominating requirement has to do with grain alignment. For example in the Ag-clad Bi:HTSC wires, alignment seems to take place when the superconductor "thickness" is less than about 50 μm. The following account demonstrates that this is certainly compatible with flux jump stability.

In calculating the filament diameter requirements for flux jump stability two alternative criteria may be applied -- the adiabatic and the dynamic. The former dominates if the heat capacity is high and cryocooling can be ignored; in the dynamic case heat conduction to a cryogen bath must be invoked. The maximum filament diameter under the adiabatic criterion (based on a slab calculation[12, p.134]) in c.g.s. units is

$$d_{ad} = \sqrt{10^9\left(\frac{3}{\pi}\right)C(T)\Delta T_0/J_c(T,H)} \qquad (7)$$

The dynamic criterion (based on a cylinder calculation[12, p.156]) yields

$$d_{dyn} = 2\sqrt{8\frac{K_{SC}}{\rho_{Ag}}\Delta T_0\frac{1-\lambda}{\lambda}}\ /J_c(T,H) \qquad (8)$$

In these equations C(T) and K_{SC} are the heat capacity and thermal conductivity, respectively, of the superconductor (SC), ρ_{Ag} is the silver stabilizer resistivity, λ is the volume fraction of SC in the composite (herein 0.5) and $\Delta T_0 \equiv J_c/(-dJ_c/dT)$.

The equations can be evaluated using the appropriate cryophysical property data.

Cryophysical Property Data

The temperature dependencies of the relevant thermal and electrical properties of YBCO and copper (for model calculations of the stabilities of YBCO/Cu composites) were previously listed.[5] In what follows we repeat some of the earlier calculations but for the more realistic case of YBCO/Ag, since the following data for Ag has recently become available. In addition, for ΔT_0 and $J_c(T,H)$ we draw on new data from Maley et al.[6] As indicated earlier the $J_c(T,H)$ of melt processed YBCO (T_c = 90 K) is well described by an exponentially decreasing temperature dependence to about 80 K of the form (5.92 x 10^5 A/cm^2)exp(-T/T_s) with T_s = 19.87 K, combined with a Kim-type field dependence quotient of the form $H_0(T)/\{H_0(T)+H\}$ in which $H_0(T) = a\text{-}bT$ (a = 2.504 tesla, b = 2.79x10^{-2} tesla/K). Above about 80 K, J_c drops linearly to zero at T_c. Thus at 4 K, $\Delta T_0 = T_s$ = 19.87 K; while at 77 K, ΔT_0 may be approximated by the usual (T_c-T_b) = 13 K.

Electrical Resistivity of the Silver Stabilizer: Drawn wires of 99.99% Ag and an Ag-0.1%Al alloy were annealed in air for 24h/840°C during which they became charged with oxygen and the alloy internally oxidized to Ag plus Al_2O_3. Their measured resistivities were: **Ag:** ρ_{4K} = 9.27 nΩcm, ρ_{77K} = 290.56 nΩcm; **Ag+Ox:** ρ_{4K} = 247.42 nΩcm, ρ_{77K} = 624.51 nΩcm.

Magnetoresistance of Silver: The magnetoresistivity of Ag over the temperature range 4.2-159 K has been measured by Iwasa et al.[13] Based on their data we have deduced that at 4.2 K a field of 5 T adds to Ag a resistivity of 11.61 nΩcm. In the stability calculations we assume this to be temperature independent and add it to both the 4.2 K and 77 K resistivities to take into account the effect of a 5 T field.

Maximum Filament Diameters for Flux Jump Stability

Based on Eqns. (8) and (9) the maximum filament diameters for adiabatic and dynamic flux jump stability, respectively, are as depicted in Table 1. The table indicates that at 4 K the dynamic criterion applied to the pure-Ag-stabilized composite guarantees the stability of filaments of the size expected in practice (certainly less than 100 μm). Some dynamic stability is lost when oxide-strengthened Ag is employed, in which case the adiabatic and dynamic results are similar. At 77 K both YBCO and YBCO/Ag are "overstable" from both adiabatic and dynamic standpoints; filaments thicker than those that would ever be encountered in practice are immune to flux jumping.

Table 1. Maximum Filament Diameters for Adiabatic and Dynamic Stability

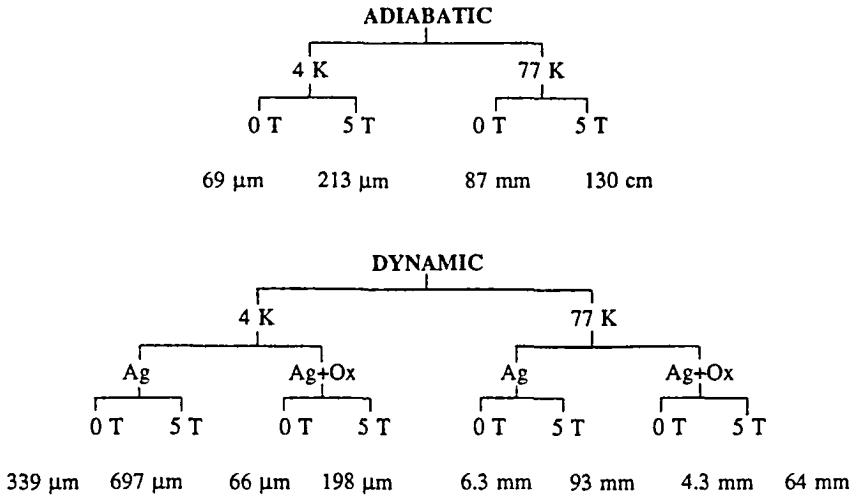

Strand Stability and Cryostability

Other aspects of strand stability, including maximum adiabatic strand diameter and cryostability have been adequately explored in an earlier publication.[5] An important feature of strand cryostability is the possibility of occurrence, as the result of some disturbance, of the "minimum propagating zone" or MPZ, and the rate at which it expands (v_{MPZ}) to quench (and thereby protect) the coil in which it was imbedded. In the reference just cited it is clear that at 77 K the adiabatic v_{MPZ} is so slow that special precautions must be taken to avert hot-spot formation and possible strand burn-out.

AC LOSS

Hysteretic and Eddy Current Loss in HTSC/Ag MF Strands

At low temperatures the attractive characteristic of the HTSC is its high upper critical field. Since advantage would not be taken of this property in an AC application it is doubtful if HTSCs would ever replace LTSCs in such conditions. For this reason we confine our analysis of AC loss to the high temperature regime around 77 K.

According to the Carr's "anisotropic-continuum" representation of a multifilamentary superconductor[14] the AC loss experienced by a superconducting strand in a transverse magnetic field consists of two components -- hysteretic (a property of the irreversible superconductor itself) and eddy current (due to currents circulating around the composite). At low frequencies of the applied magnetic field the hysteretic component in c.g.s practical units is given by

$$\dot{Q}_h = \frac{8x10^{-8}}{3\pi}\lambda J_c d\, H_m f \qquad W/cm^3 \qquad (10)$$

where H_m is the amplitude of a sinusoidal field of frequency f. Again at low frequencies the eddy current component is given by

$$\dot{Q}_e = \frac{10^{-7}}{2}\frac{L_p^2}{\rho_{\perp n\Omega cm}} H_m^2 f^2 \qquad W/cm^3 \qquad (11)$$

where L_p is the twist pitch and $\rho_{\perp n\Omega cm}$ is the transverse resistivity of the strand in nΩcm (which in this case we will take to be the matrix (Ag) resistivity). To provide an estimate of the magnitudes of these quantities to be expected in a typical situation, we imagine fields of amplitudes, H_m, of up to 800 Oe, to be applied to a series of typical MF strands.

Our basic model MF strand is in the form of a central filament surrounded in succession by rings of 6, 12, and 18 filaments. A double-stack strand is composed of a six-around-one bundle of the above, for a total of (1+6+12+18)x7 = 259 filaments. Let strands of 1, 7, 19, 37, and 259 filaments of $J_c(0T) = 1.228 \times 10^4$ A/cm^2 each carry a critical transport current of 10 A. The corresponding filament diameters under these conditions would then be 322, 122, 74, 53, and 20 μm -- a realistic sequence. The H_m-proportional hysteretic power loss would then be as depicted in Fig. 6.

To model the eddy current loss we equate $\rho_\perp$ with the 77 K resistivity of oxidized Ag-0.1%Al, viz. 624.51 nΩcm, and assume twist pitches, L_p, of 1, 0.5, and 0.25 cm. The corresponding eddy current power loss is also depicted in Fig. 6. The maximum possible eddy current loss occurs when the filaments are all fully coupled. In this case Q_e is equivalent to the hysteretic loss of a monocore of critical current density λJ_c equal in diameter, D, to that of the whole filamentary bundle. Obviously the ratio $Q_{coupled}/Q_{monocore}$ is just $Q_{coupled}\sqrt{\lambda}$. Represented by the dashed line in Fig. 6 it places a limit on the magnitude of the low frequency eddy current loss. The possibility of eddy current loss is most serious in strands with very large numbers of fine filaments -- e.g. those intended for LTSC accelerator magnet windings. But even in the present example, for H_m = 800 Oe, the ratio of Q_e(most strongly coupled) to Q_h(finest filaments) is 94.9/4.2 = 22/1.

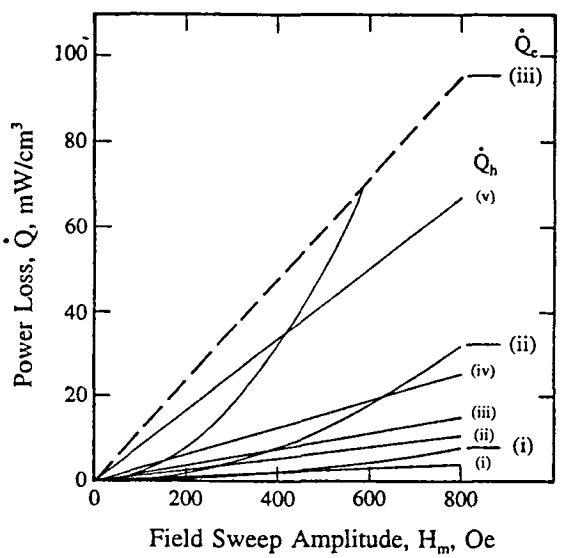

Figure 6. Per-unit-volume AC loss for a series of model MF YBCO/Ag strands of fixed λ (= 0.5) and I_c (= 10 A), hence fixed SC area, but with filament numbers/diameters of: (i) 259/10 μm, (ii) 37/26 μm, (iii) 19/36 μm, (iv) 7/60 μm, and (v) 1/158 μm. Depicted is the hysteretic loss, $\dot{Q}_h$, and the eddy current loss, $\dot{Q}_e$, corresponding to strand twist pitches, L_p, of (i) 0.25, (ii) 0.5, and (iii) 1 cm. Also shown as a dashed line is the limiting eddy current loss, that for a fully coupled strand, equal to $\dot{Q}_{h,monocore}/\sqrt{\lambda}$. The Q_h data are valid for H_m greater than the full penetration fields of: (i) 10, (ii) 26, (iii) 36, (iv) 60, and (v) 158 Oe.

Twist Pitch, Matrix Resistivity, and Filament-Diameter Considerations

Based on the above physical-property data set the ratio Q_e/Q_h is just $0.7681(L_p^2/d_{\mu m})H_m$ which emphasizes the importance of reducing both twist pitch and filament diameter in the minimization of eddy current loss. For equal loss at H_m = 500 Oe, for example, $d_{\mu m}$ = 384 $L_{p,cm}^2$. When d = 24 μm this calls for a twist pitch of 0.25 cm. For the strand diameter $D = d\sqrt{(N/\lambda)}$ = 0.46 mm considered in these examples, this corresponds to a pitch/diameter ratio of 5.5/1 which would be quite tight even for a NbTi/Cu strand. The alternative to reducing L_p is increasing the matrix resistivity.

If sufficient twist or resistivity cannot be introduced, full electrical advantage cannot be taken of multifilamentary subdivision, especially since fine filaments often turn out to be interconnected by "bridges". Nevertheless there are other advantages to be considered: (1) Reduction of filament diameter aids in HTSC grain alignment. (2) The ductile interfilamentary matrix with its crack-stopping potential can be expected to contribute a higher strain tolerance to the finer-filament composite; in which case even bridging may be an advantage.

REFERENCES

1. S.W. Hsu, K. Chen, and W.H. Lee, "Temperature and Field Sweeping Rate Dependence of Flux Jumps in a Melt-Textured $YBa_2Cu_3O_{7-x}$ Superconductor" **75**, 799-803 (1990).
2. K.-H. Müller and C. Andrikidis, "Flux Jumps in Melt-Textured Y-Ba-Cu-O", Phys. Rev. B. **49**, 1294-1306 (1994).
3. R. Hancox, "The Superconductivity of Sintered Nb_3Sn at Temperatures Above 4.2 K", Appl. Phys. Lett. 7, 138-139 (1965).
4. J. Sosnowski, "Influence of Magnetic History on Flux Jump Fields", J. Appl. Phys. **59**, 4189-4191 (1986).
5. E.W. Collings, "Conductor Design with High-T_c Ceramics: A Review", **Advances in Superconductivity-II**, ed. by T. Ishiguro and K. Kajimura, (Springer-Verlag, 1990) pp. 327-333.
6. P.J. Kung, M.P. Maley, M.E. McHenry, J.O. Willis, J.Y. Coulter, M. Murakami, and S. Tanaka, "Magnetic Hysteresis and Flux Creep of Melt-Powder-Melt-Growth $YBa_2Cu_3O_7$ Superconductors", Phys. Rev. B. **46**, 6427-6434 (1992).
7. M. Chiba, T. Ogasawara, N. Miyazawa, S. Ban, et al, "The Magnetic Stability of Face-Cooled Composite Tape Superconductors", IEEE Trans. Magn. **27**, 1656-1659 (1991).
8. H. Brechna, **Superconducting Magnet Systems**, (Springer Verlag, NY, 1973) pp. 139-142; see also H. Brechna, "Superconducting Magnets", in **Superconducting Machines and Devices, Large Systems Applications**, ed. by S. Foner and B. Schwartz, NATO Advanced Study Series, (Plenum Press, NY, 1974) pp. 162-165.
9. M.N. Wilson, **Superconducting Magnets**, (Oxford, NY, 1983) pp. 41-46.
10. S. Timoshenko and J.N. Goodier, **Theory of Elasticity**, (McGraw Hill, NY, 1951), pp. 69-71.
11. K. Salama, private communication, 1994.
12. E.W. Collings, **Applied Superconductivity, Metallurgy and Physics of Titanium Alloys**, Volume 2, (Plenum Press, NY, 1986).
13. Y. Iwasa, E.J. McNiff, R.H. Bellis, and K. Sato, "Magnetoresistance of Silver over Temperature Range 4.2 - 159 K", Cryogenics **33**, 836-838 (1993).
14. W.J. Carr Jr., **AC Loss and Macroscopic Theory of Superconductors**, (Gordon and Breach, NY, 1983) p. 348.